Highly Efficient Fe-N-C Nanoparticles Modified Porous Graphene Composites for Oxygen Reduction Reaction

Yan Zhang,[1] Lei Qian,[1,z] Wen Zhao,[1] Xiaomin Li,[1] Xiaoshuai Huang,[1] Xianmin Mai,[2,z] Zhikang Wang,[3] Qian Shao,[4] Xingru Yan,[5] and Zhanhu Guo ⬤[5,*,z]

[1]*Key Laboratory for Liquid-Solid Structural Evolution and Processing of Materials (Ministry of Education), Shandong University, Jinan 250061, People's Republic of China*
[2]*School of Urban Planning and Architecture, Southwest Minzu University, Chengdu 610041, People's Republic of China*
[3]*College of Eco-environmental Engineering, Guizhou Minzu University, Guiyang, Guizhou, 550025, People's Republic of China*
[4]*College of Chemical and Environmental Engineering, Shandong University of Science and Technology, Qingdao 266590, People's Republic of China*
[5]*Integrated Composites Laboratory (ICL), Department of Chemical & Biomolecular Engineering, University of Tennessee, Knoxville, Tennessee 37996, USA*

Iron-nitrogen-carbon nanoparticles modified porous graphene (Fe-N-C/PGR) was synthesized from the pyrolysis of porous freeze-dried composites of iron (II) phthalocyanine (FePc) nanoclusters and graphene oxide (GO). By pyrolysis in argon atmosphere, the GO was reduced into graphene (GR), and the FePc nanoclusters were converted to Fe-N-C nanoparticles on the GR surface. The morphologies and composition of the resulted Fe-N-C/PGR composites were characterized by field emission scanning electron microscopy, transmission electron microscopy, X-ray diffraction, X-ray photoelectron spectroscopy and Raman spectra. The Fe-N-C/PGR composites exhibited three-dimensional interpenetrated porous structure, and many particles with Fe-N-C active sites were distributed on the GR nanosheets. Electrocatalytic properties of the Fe-N-C/PGR composites were investigated by cyclic voltammetry and linear sweep voltammetry. For the Fe-N-C/PGR composites with 3:1 mass ratio of FePc nanoclusters to GO precursor, it showed the highest electrocatalytic activity with the peak current density of 5.82 mA cm^{-2} at −0.39 V, which was ascribed to the synergistic effect of Fe-N-C active sites and PGR with good porous structures. The electron transfer number of 3.94 for the Fe-N-C/PGR composite indicated a direct 4-electron pathway for the ORR. Furthermore, the Fe-N-C/PGR composites showed high stability and better tolerance to methanol than the commercial 20% Pt/C catalysts.
© 2018 The Electrochemical Society. [DOI: 10.1149/2.0991809jes]

Oxygen reduction reaction (ORR) is a key process in energy conversion systems such as fuel cells and metal-air batteries. However, the sluggish ORR kinetics usually needs be catalyzed by high efficient catalysts to boost the performance of fuel cells.[1–3] Although Pt-based materials are the most commonly used ORR cathode catalysts due to their high activity, they suffer from high cost, rare resource and easy poisoning.[4–6] Thus, it is very necessary to develop nonprecious metal ORR catalysts with low cost, high catalytic activity and durability, which can replace the precious Pt-based catalysts.

Numerous nonprecious metal catalysts for ORR have been investigated over the last several decades, such as nitrogen or sulfur doped carbon materials,[7,8] transition metal oxides,[9] metal chalcogenides,[10,11] and metal-N$_4$ macrocyclic compounds.[12–14] Since the cobalt phthalocyanine was investigated as ORR catalysts by Jasinski in 1964,[15] metal-N$_4$ macrocyclic compounds including pophyrins and phthalocyanine have been extensively investigated. Among these metal-N$_4$ macrocyclic compounds, iron (II) phthalocyanine (FePc) has shown excellent electrocatalytic performance toward ORR.[16,17] In addition, FePc is inexpensive or easy to prepare with abundant sources. Thus, FePc is considered to be the most promising alternative nonprecious metal catalysts toward ORR. Although FePc shows good electrocatalytic performance toward ORR, its conductivity, stability and electrocatalytic activity still need be further improved.[18,19] Therefore, in order to enhance the electrocatalytic activity and stability of FePc for ORR, heat-treatment in an inert atmosphere at high temperature is usually applied.[20–23] During the heat-treatment process, the FePc molecules are effectively transformed into a large number of Fe-N-C structure as the active sites for the ORR, resulting in the improved stability[24,25] and catalytic activity (8 mA cm^{-2} at 1600 rpm in 0.1 M KOH).[26]

Numerous carbon materials have been investigated as the supports, such as carbon powders, carbon nanotubes and graphene (GR).[27–41]

Among these, GR has many unique properties, including high electrical conductivity, large specific surface area and good chemical stability.[42–46] However, the GR suffers from aggregation due to the π-π interaction and Van der Waals force between GR sheets, which reduces the specific surface area. Therefore, three-dimensional GR networks have attracted considerable attention.[47,48] By building three-dimensional network structures, the aggregation of GR sheets is effectively avoided. For example, Yin et al.[49] synthesized a hybrid of nitrogen-doped GR aerogel supported FeN$_x$ nanoparticles by a two-step hydrothermal process with a comparable catalytic activity (about 5.7 mA cm^{-2} at 1600 rpm in 0.1 M KOH) to the commercial Pt/C catalyst. Yu et al.[50] prepared Fe-N-C modified GR sponge catalysts by hydrothermal and pyrolysis processes, the obtained Fe-N-C catalysts exhibited excellent ORR and oxygen evolution reaction catalytic performance, with a discharge capacity of 6762 mAh g^{-1} used as the cathode for lithium-air batteries. However, most of the recently reported catalysts have been prepared by hydrothermal method and the Fe-N-C active sites are not easy to adjust. Therefore, a facile and effective route is still desirable for the synthesis of a Fe-N-C supported GR catalyst.

Porous graphene (PGR) prepared by facile freeze-drying method has been used to support Pt nanoparticles to serve as excellent ORR catalysts.[51] The PGR had a large specific surface area, porous structure, high electrical conductivity and good stability, which offered many exposed active sites, fast electron transfer pathway and mass transport during the ORR process. It can be an ideal support for the Fe-N-C active sites as ORR catalyst. FePc nanoclusters modified GR composites have been recently prepared and showed promising catalytic performance for ORR.[52] However, due to poor conductivity and instability of FePc, its catalytic activity for ORR still needs further improvement.

In this work, Fe-N-C nanoparticles modified PGR catalysts (Fe-N-C/PGR) were prepared by a facile freeze-drying method followed by thermal treatment in argon atmosphere, as illustrated in Fig. 1. FePc nanoclusters were used as the precursor to produce Fe-N-C nanoparticles and tune the content of Fe-N-C active sites by changing the FePc

*Electrochemical Society Member.
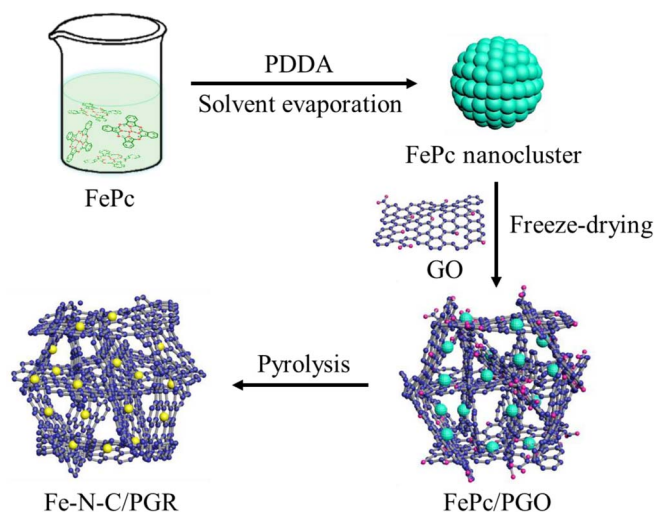zE-mail: qleric@sdu.edu.cn; maixianmin@foxmail.com; zguo10@utk.edu

Figure 1. The schematic representation for preparation of the Fe-N-C/PGR composites.

nanocluster amount. Field-emission scanning microscopy (FESEM), transmission electron microscopy (TEM), X-ray diffraction (XRD), X-ray photoelectron spectroscopy (XPS) and Raman spectra were used to characterize and investigate the morphologies, microstructures and composition of the resulted Fe-N-C/PGR. Their electrocatalytic properties of ORR activity, mechanism, stability and tolerance to methanol were also studied in details by the measurements of cyclic voltammetry (CV) and linear sweep voltammetry (LSV).

Experimental

Chemicals and reagents.—GO was purchased from Nanjing Ji-cang Nano Tech. Co. Ltd. FePc, poly(diallyldimethlammonium chloride) (PDDA, 20 wt% in water) and Nafion (5% in a mixture of lower aliphatic alcohols and water) were obtained from Sigma-Aldrich. 20% Pt/C was bought from Alfa Aesar (China) Chemicals Co., Ltd. All other reagents and chemicals were analytical grade and used without further purification. Deionized water was used to prepare all the solutions.

Preparation of Fe-N-C/PGR composites.—FePc nanoclusters were prepared according to our reported method.[52] Briefly, 80 mL FePc dispersion solution (4 mg mL^{-1} in ethanol) was added into 0.1% PDDA solution (20 mL) slowly under magnetic stirring. The mixed dispersion was magnetically stirred at room temperature continuously. When ethanol was completely evaporated, the mixture was centrifuged and washed with deionized water three times. The obtained precipitate was dried in an oven at 80°C to produce the FePc nanoclusters.

The FePc nanoclusters and GO were respectively dispersed in deionized water (4 mg mL^{-1}) by ultrasonication. The homogeneous FePc nanoclusters and GO dispersion in a volume ratio of 1:7 were mixed by ultrasonication. The resulted dispersion was put into liquid nitrogen until the dispersion was almost frozen, and then it was quickly put into a freeze drier for 36 h, in which the ice was removed by sublimation to produce FePc nanoclusters loaded porous GO composites. The composites were annealed at 750°C in argon atmosphere for 2 h with a heating rate of 5°C/min, and the Fe-N-C/PGR (1:7) composites were obtained after the heat-treatment. The PGR, Fe-N-C/PGR (1:3), Fe-N-C/PGR (1:1) and Fe-N-C/PGR (3:1) composites were also prepared using the same method as the composites with different mass ratios of the FePc nanoclusters to GO.

Preparation of Fe-N-C/PGR composite modified electrode.—The Fe-N-C/PGR composites were dispersed into 0.5% Nafion to obtain 10 mg mL^{-1} dispersion. 5 μL Fe-N-C/PGR dispersion was dropped onto the cleaned glassy carbon electrode (GCE) or rotating disk electrode (RDE) and dried at room temperature to prepare the modified working electrode. The loading amount of the Fe-N-C/PGR composites was about 714.3 μg cm^{-1}. Before modification, the GCE was firstly polished carefully using 1.0, 0.3, and 0.05 μm α-Al$_2$O$_3$ powders, then cleaned with ethanol and deionized water at least three times, respectively. Before electrocatalytic measurements, it is required to purge the electrolyte solution with O$_2$ for 30 min to ensure the oxygen saturation.

Characterizations.—Morphology and structure of the Fe-N-C/PGR composites were recorded by a SU-70 FESEM at 15 kV (Hitachi, Tokyo, Japan) and Tecnai G2 F20 TEM (FEI, America, operating at 200 kV). XRD measurement was performed on an XD-3 X-ray diffractometer operated at 36 kV and 20 mA using Cu Kα radiation. XPS was performed on a ThermoFisher with Al Kα as the excitation source (200 eV). Raman spectra were performed in a Raman spectroscopy (Renishaw, inVia) with a wavelength laser of 532 nm.

Electrochemical experiments were investigated by a CHI 660D electrochemical workstation (Shanghai ChenHua Instruments Co., Ltd.) and an LK 5100 electrochemical luminescence analysis system (Tianjin LanLiKe chemical high electronic technology Co., Ltd) in oxygen-saturated electrolyte solutions at room temperature. A three-electrode electrochemical cell was used for the electrochemical experiments, in which a modified GCE (3 mm diameter) or RDE (carbon, 3 mm diameter) served as the working electrode, a platinum wire used as auxiliary electrode, and an Ag/AgCl (saturated KCl) electrode as reference. Electrocatalytic activity toward ORR of the resulted Fe-N-C/PGR was investigated by electrochemical experiments.

During the ORR process, the number of electrons transferred per oxygen molecule on Fe-N-C/PGR (3:1) composites electrode was evaluated by the K-L equation as follows:[29,30]

$$\frac{1}{j} = \frac{1}{j_K} + \frac{1}{j_L} = \frac{1}{B\omega^{1/2}} + \frac{1}{j_K} \quad [1]$$

$$B = 0.2nF(D_{O_2})^{2/3}v^{-1/6}C_{O_2} \quad [2]$$

$$j_K = nFkC_{O_2} \quad [3]$$

where j represents the measured current density, j_K, and j_L are the kinetic and diffusion limiting current densities, respectively; ω is the rotating speed of RDE (rpm); the constant 0.2 is adopted when the rotating speed is expressed in rpm; n represents the number of electrons transferred during ORR process; F is the Faraday's constant (F = 96485 C mol^{-1}); D_{O_2} is the diffusion coefficient of O$_2$ in 0.1 M KOH solution (1.9×10^{-5} cm^2 s^{-1}); v is the kinetic viscosity of O$_2$ (0.01 cm^2 s^{-1}); C_{O_2} is the bulk concentration of O$_2$ (1.2×10^{-6} mol cm^{-3}); and k is the electron transfer rate constant. The number of electrons transferred during ORR was extracted by the slope of K-L plots (j^{-1} vs. $\omega^{-1/2}$) based on the LSV date.

Results and Discussion

Morphology of Fe-N-C/PGR composite.—The morphologies of the Fe-N-C/PGR composites were examined by FESEM and TEM. From the FESEM images as shown in Figs. 2a–2d, all the four materials are observed to have 3D interpenetrating porous structure constructed by the wrinkled GR sheets. This structure was formed in the freeze-drying process, in which ice crystals were produced, and the GO sheets were excluded and assembled between the ice crystals. The 3D porous GO (PGO) was produced when the ice crystals were sublimated. After the subsequent thermal treatment, the PGO was reduced to PGR by removing the oxygen-containing functional groups and its interpenetrating porous structure was remained. Figs. 2a and 2b shows the morphology of Fe-N-C/PGR (1:7) and Fe-N-C/PGR (1:3) composites respectively. No obvious Fe-N-C particles were observed on the PGR of the Fe-N-C/PGR (1:7) composites, and only few small
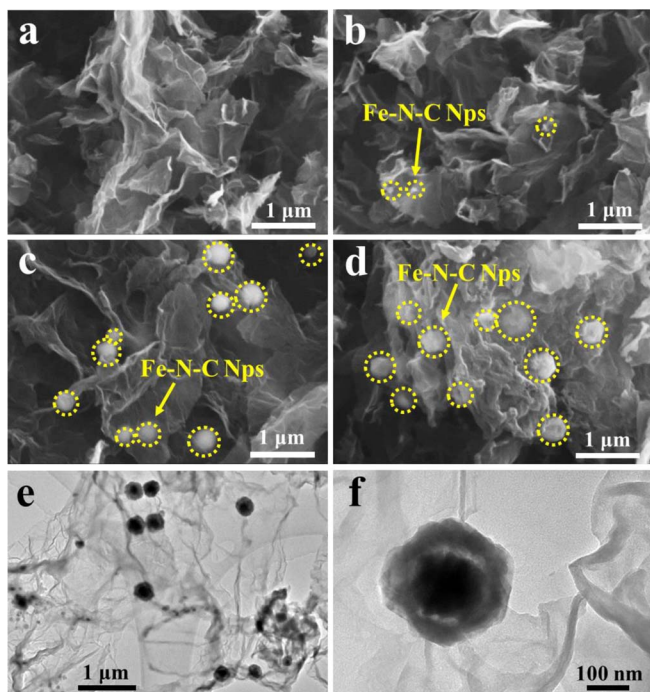
Figure 2. FESEM images of (a) Fe-N-C/PGR (1:7); (b) Fe-N-C/PGR (1:3); (c) Fe-N-C/PGR (1:1) and (d) Fe-N-C/PGR (3:1) composites; TEM images of (e and f) Fe-N-C/PGR (3:1) composites.

particles appeared on the PGR surface of Fe-N-C/PGR (1:3) composites. It was possibly attributed to the low content of FePc nanoclusters. However, for the Fe-N-C/PGR (1:1) and Fe-N-C/PGR (3:1) composites (Figs. 2c and 2d) with higher contents of FePc nanoclusters, many particles (~ 300 nm) were loaded on the surface of GR sheets derived from the pyrolysis of FePc nanoclusters. The FePc nanoclusters were supported on GO through electrostatic interaction between PDDA and carboxyl groups on GO surface. And by the subsequent heat-treatment in argon atmosphere, the FePc nanoclusters were converted into many particles containing a large number of Fe-N-C active sites. Figs. 2e and 2f shows the detailed microstructure of Fe-N-C/PGR (3:1) composites as observed by TEM. Many Fe-N-C nanoparticles with different sizes were closely stacked on the very thin wrinkled GR nanosheets (Fig. 2e). This observation is consistent with that observed by FESEM. In addition, the Fe-N-C nanoparticles with the size of about 300 nm are observed to display a spherical structure with a thicker solid core ($\sim$150 nm) and thinner shell about 70 nm (Fig. 2f).

Structure and composition of Fe-N-C/PGR composites.—Fig. 3a shows the XRD patterns of the as-prepared Fe-N-C/PGR composites. The observed peak at about $25.5°$ among all the four catalysts corresponds to the (002) plane of graphitic carbon, indicating the presence of graphitic structure and the reduction of GO into GR by thermal treatment in argon atmosphere. With increasing the content of Fe-N-C structure, several peaks appeared more clearly in the Fe-N-C/PGR (1:1) and Fe-N-C/PGR (3:1) composites. The peak at $35.5°$ corresponds to the (111) plane of FeN (PDF. NO. 50-1087). The FeN might be derived from the decomposition of FePc nanoclusters during the pyrolysis process.[22,49] Besides, the Fe_3N (111) (PDF. NO.49-1662) was observed in the peak at $43.4°$. The diffraction peak appeared at $44.7°$ could be attributed to the (031) plane of Fe_3C (PDF. NO.35-0772). It was proposed that when phthalocyanine ring was decomposed, some Fe atoms might be released and probably coordinated with the rich N or C sources to form the Fe_3N and Fe_3C, while the detailed formation process still needs further investigation. From these results, the $Fe-N_x$ phase and Fe_3C were successfully formed in the Fe-N-C/PGR composites during heat-treatment.[49,53]

The chemical elements of the Fe-N-C/PGR (3:1) composites were evaluated by XPS. The corresponding C_{1s}, N_{1s} and Fe_{2p} spectra are shown in Figs. 3b, 3c and 3d, respectively. As shown in Fig. 3b, three types of carbon species including C=C (284.59 eV), C-N (284.76 eV) and C=N (288.39 eV) are observed. No observation of carbon states of C=O, C-OH, C-O-C or O-C=O derived from oxygen-containing functional groups indicates that the GO was reduced to GR. The N_{1s} spectra were fitted into four different peaks at 398.19, 399.19, 400.4 and 400.9 eV (Fig. 3c), corresponding to pyridinic N (48.67%), Fe-N (15.03%), pyrrolic N (10.49%) and graphitic N (25.82%), respectively.[54–57] It has been reported that the pyridinic N played a significant role in the formation of Fe-N-C active sites, and was able to coordinate with Fe ions due to the lone pair electrons.[58] The presence of Fe-N peak also indicates that the Fe ions were probably coordinated with pyridinic N to form Fe-N-C active sites. Two observed peaks at 711.09 and 723.86 eV correspond to $Fe^{2+}_{2p1/2}$ and $Fe^{2+}_{2p3/2}$ from the Fe_{2p} binding energy, and are attributed to the Fe^{2+} in Fe-N-C structure. The peak position was consistent with that reported in the literatures of Fe-N-doped carbon nanotube and porous carbon supported Fe-N-C composite.[25,59]

Fig. 4 shows the Raman spectra of the Fe-N-C/PGR nanocomposites. All the four Fe-N-C/PGR composites displayed the characteristic D and G bands at around 1350 and 1590 cm^{-1}, respectively. The intensity ratio of the D band and G band (I_D/I_G) was often allowed to estimate the disordered degree from the graphitic structure of carbon materials.[21,44] The I_D/I_G for Fe-N-C/PGR (1:7), Fe-N-C/PGR (1:3), Fe-N-C/PGR (1:1) and Fe-N-C/PGR (3:1) composites was 0.79, 0.86, 0.92 and 0.89, respectively. The Fe-N-C/PGR (1:7) and Fe-N-C/PGR (1:3) composites had the lower I_D/I_G ratios, corresponding to the existence of more graphited carbon. It was resulted from the relatively high content of PGR. While for the Fe-N-C/PGR (1:1) and Fe-N-C/PGR (3:1) composites, the I_D/I_G values were increased slightly. This confirmed that the Fe-N-C/PGR (1:1) and Fe-N-C/PGR (3:1) composites had more defects and disordered carbon. It was attributed to the higher content of Fe-N-C nanoparticles derived from the FePc nanoclusters.

Electrocatalysis of Fe-N-C/PGR composite for ORR.—To investigate the electrocatalytic activity of Fe-N-C/PGR composites, the CV measurements were carried out in an alkaline medium. Fig. 5a shows the CV curves of PGR, Fe-N-C/PGR (1:7), Fe-N-C/PGR (1:3), Fe-N-C/PGR (1:1) and Fe-N-C/PGR (3:1) composites modified GCE in O_2 saturated 0.1 M KOH at a scan rate of 10 mV s^{-1}. The Fe-N-C/PGR composites all are observed to exhibit well-defined reductive peaks in the range of -0.35 and -0.4 V, which are more positive than those (from -0.4 to -0.45 V) of pure PGR. Compared with the PGR (about 1.2 mAcm^{-2}), the peak current densities of Fe-N-C/PGR composites were also improved (about 3.4 to 5.82 mA cm^{-2}). It indicated that the Fe-N-C/PGR composites exhibited much better electrocatalytic performance than pure PGR toward ORR. We also investigated the ORR electrocatalytic activity of Fe-N-C/PGR composites with different mass ratios of FePc nanoclusters to GO precursor. It was found that the obtained Fe-N-C/PGR (3:1) composites showed the highest reductive peak current density (5.82 mA cm^{-2} at -0.39 V) for ORR. Although the peak potentials of Fe-N-C/PGR (1:7) and Fe-N-C/PGR (1:3) composite were a little more positive (-0.38 and -0.35 V), they exhibited low peak current densities of 3.4 and 4.8 mA cm^{-2}, respectively. Furthermore, The Fe-N-C/PGR (1:1) composites showed not only low peak current density (4.93 mA cm^{-2}) but also negative peak potential (-0.4 V). Therefore, due to the possible formation of more Fe-N-C active sites, the Fe-N-C/PGR (3:1) composites showed a reductive peak current density of 5.82 mA cm^{-2} at -0.39 V toward ORR, even much higher than other reported Fe-N-C based catalysts for ORR (about 4 mA cm^{-2} for Fe-N-doped carbon nanotube, about 2.5 mA cm^{-2} for FeN$_x$/nitrogen-doped graphene aerogel).[23–26,43] Thus, the Fe-N-C/PGR (3:1) composites were chosen for the subsequent investigations. Fig. 5b shows the CV curves from the Fe-N-C/PGR (3:1) composites in O_2 and N_2 saturated 0.1 M KOH. A reduced peak obviously appeared at about -0.4 V for the Fe-N-C/PGR (3:1) composites in the O_2 saturated 0.1 M KOH. However, for the catalysts
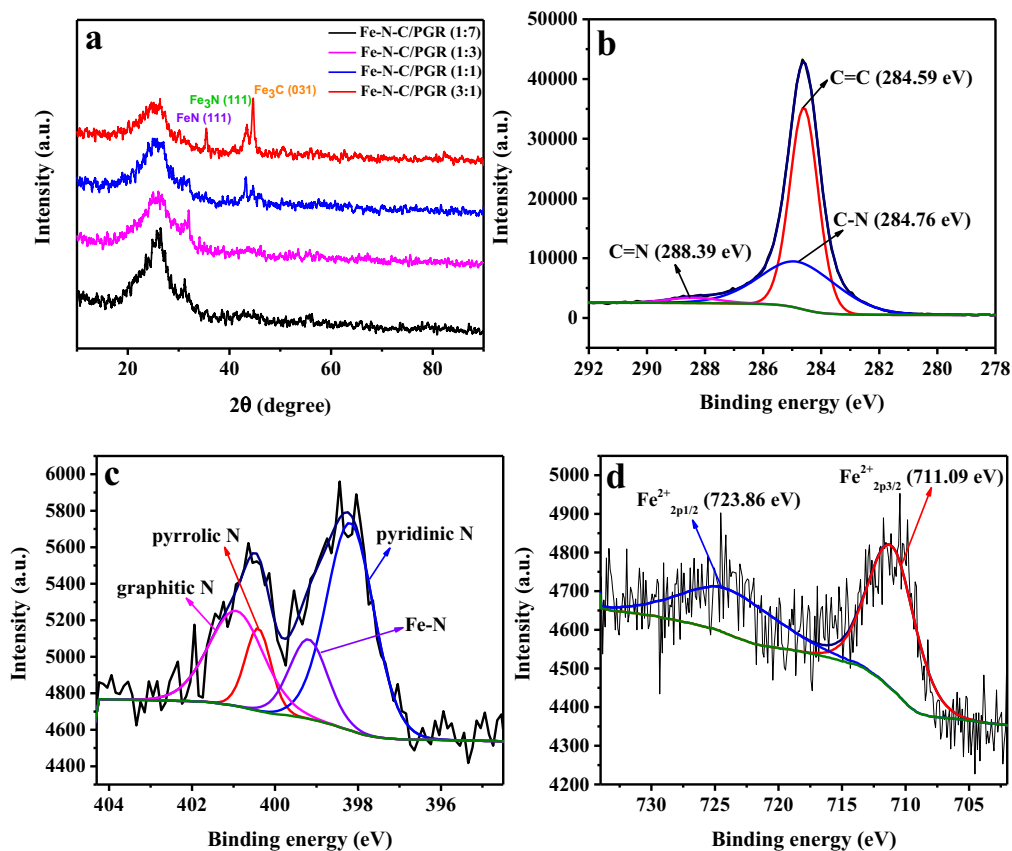
Figure 3. (a) XRD pattern of Fe-N-C/PGR (1:7), Fe-N-C/PGR (1:3), Fe-N-C/PGR (1:1) and Fe-N-C/PGR (3:1) composites; C_{1s} (b), N_{1s} (c) and Fe_{2p} (d) from the XPS spectra of Fe-N-C/PGR (3:1) composites.
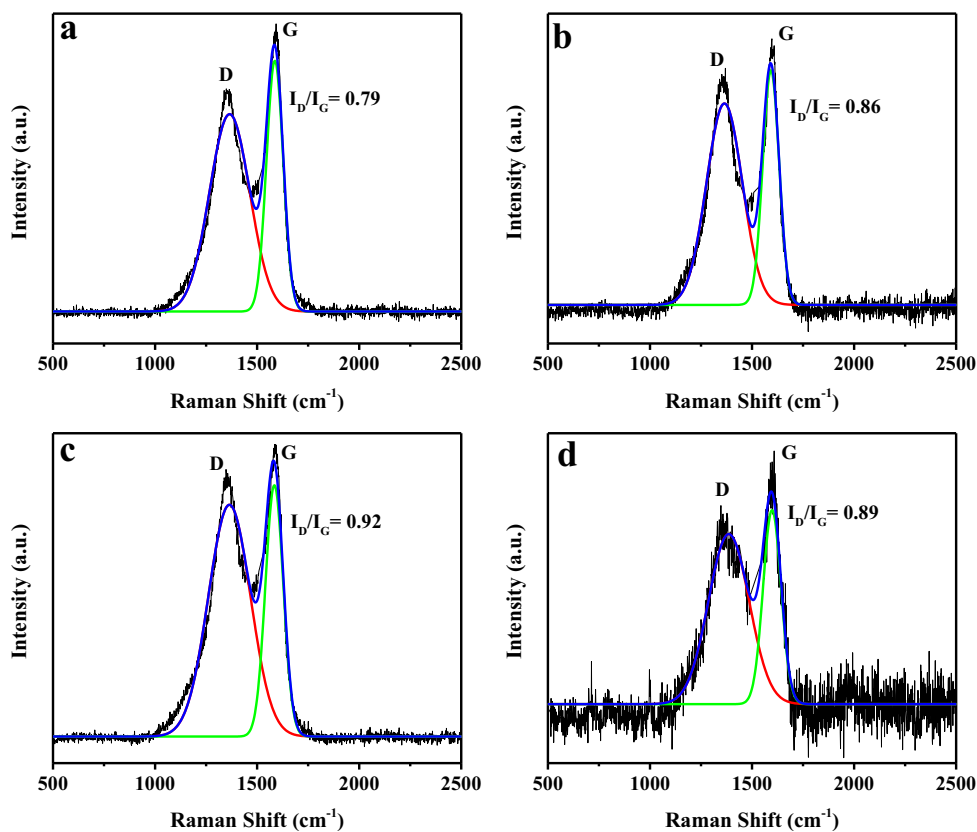

Figure 4. Raman spectra of (a) Fe-N-C/PGR (1:7); (b) Fe-N-C/PGR (1:3); (c) Fe-N-C/PGR (1:1) and (d) Fe-N-C/PGR (3:1) composites.
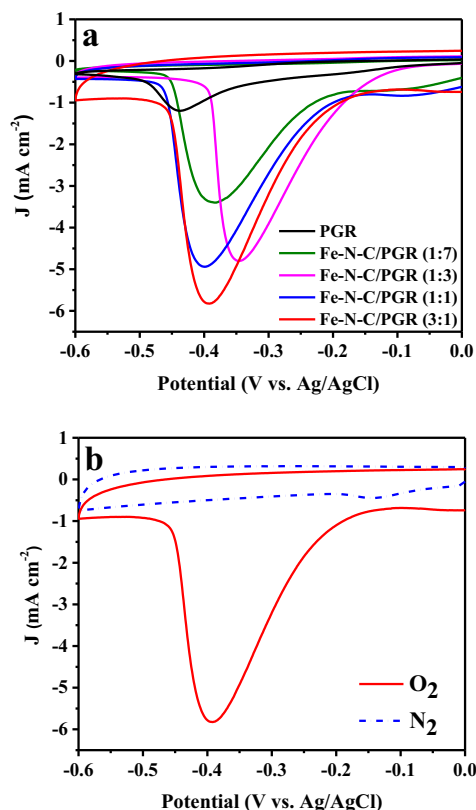
Figure 5. (a) CV curves of PGR, Fe-N-C/PGR (1:7), Fe-N-C/PGR (1:3), Fe-N-C/PGR (1:1) and Fe-N-C/PGR (3:1) composites modified GCE in 0.1 M KOH saturated with O_2 at a scan rate of 10 mV s^{-1}; (b) CV curves of the Fe-N-C/PGR (3:1) composite modified GCE in 0.1 M KOH saturated with O_2 and N_2 at a scan rate of 10 mV s^{-1}.

tested in N_2 saturated 0.1 M KOH, no peak was observed. It indicated that the reductive peak at -0.4 V for the Fe-N-C/PGR (3:1) composites was truly attributed to the ORR.

To further study the ORR mechanism of the Fe-N-C/PGR (3:1) composites, the polarization curves in the O_2 saturated 0.1 M KOH were investigated with the LSV measurements. The electron transfer number of the Fe-N-C/PGR (3:1) composites toward ORR can be calculated by Koutechky-Levich (K-L) equation, which was constructed by the polarization curves at different potentials. As is well known that in the alkaline condition, the ORR occurs either by a 4-electron pathway with the oxygen directly reduced to OH$^-$ (Eq. 4), or a 2-electron pathway with HO$_2^-$ intermediate species produced (Eq. 5).[60] In the application of fuel cells, the 4-electron direct pathway is preferred due to more efficient electron transfer and no HO$_2^-$ intermediate.

$$O_2 + 2H_2O + 4e^- \rightarrow 4OH^- \qquad [4]$$

$$O_2 + H_2O + 2e^- \rightarrow HO_2^- + OH^- \qquad [5]$$

Fig. 6a shows the obtained polarization curves of Fe-N-C/PGR (3:1) composites at different rotating speeds. It can be seen that the current density of these polarization curves was enhanced with increasing the rotating speed from 400 to 2500 rpm, which was caused by the shortened diffusion layer at high rotating speed. Fig. 6b shows the corresponding K-L plots and fitting lines of Fe-N-C/PGR (3:1) composites obtained from the polarization curves at different potentials. A good liner relationship between the K-L plots can be clearly observed, indicating the first-order reaction kinetics toward dissolved oxygen concentration as well as a similar electron transfer number. According to the slopes of K-L plots, the electron transfer numbers were evaluated to be 3.72, 4.00, 3.91 and 4.11 at -0.45, -0.5, -0.55 and -0.6 V, respectively (Fig. 6c). The average value of electron transfer number was 3.94, suggesting that the Fe-N-C/PGR (3:1) composites exhibited a direct efficient 4-electron pathway toward ORR.

The stability and tolerance to methanol have been regarded as the essential factors for evaluating the electrocatalytic performance
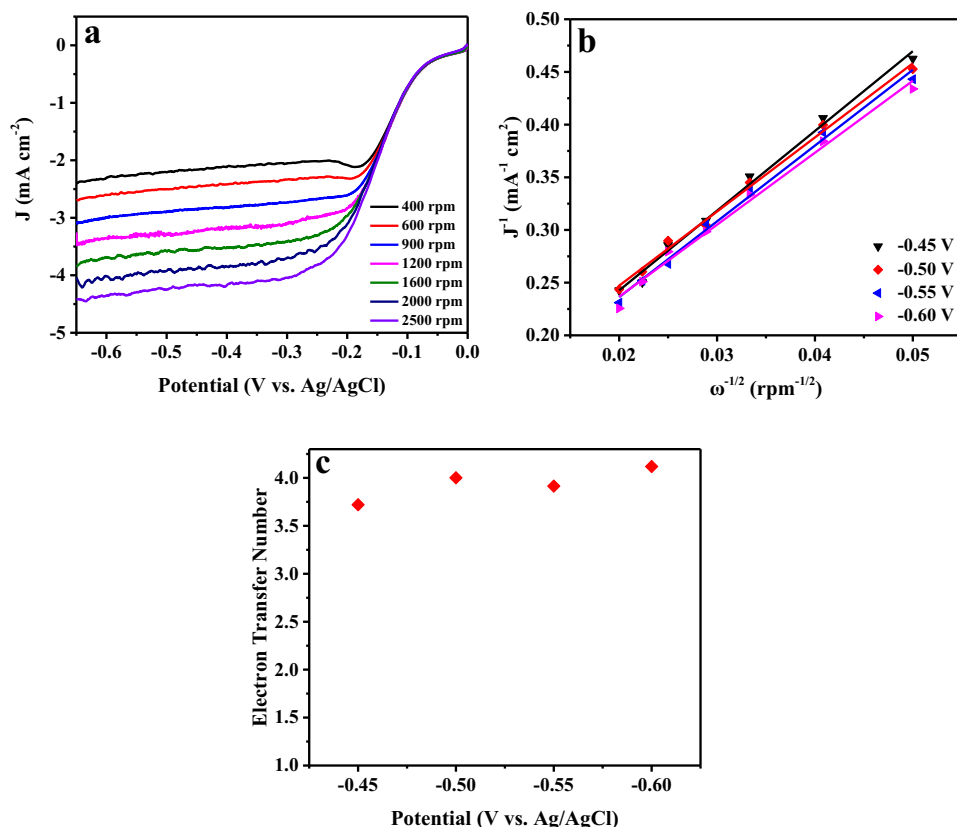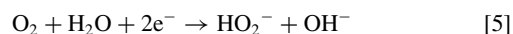

Figure 6. (a) Polarization curves of the Fe-N-C/PGR (3:1) composite modified RDE in 0.1 M KOH saturated with O_2 at different rotating speeds with a scan of 10 mV s^{-1}; (b) The Koutecky-Levich plots for the Fe-N-C/PGR (3:1) composite at different potentials between -0.45 V and -0.6 V; (c) The dependence of the electron transfer number on the potential for Fe-N-C/PGR (3:1) composites.
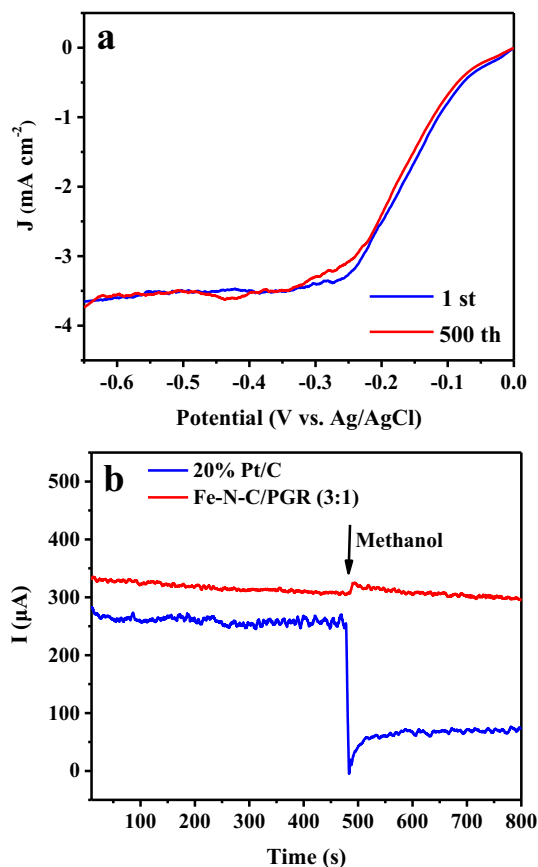
Figure 7. (a) Polarization curves of the Fe-N-C/PGR (3:1) composite modified RDE in 0.1 M KOH saturated with O_2 at 1600 rpm with a scan rate of 10 mV s^{-1} before and after 500 cycles; (b) The i-t chronoamperometric response obtained at Fe-N-C/PGR (3:1) composite and the 20% Pt/C modified RDE in 0.1 M KOH saturated with O_2 at 1600 rpm. 3 M methanol was added rapidly at about 480s.

of ORR catalysts. To explore the stability of the Fe-N-C/PGR (3:1) composites, a potential cycling of 500 cycles was operated for the Fe-N-C/PGR (3:1) composites in 0.1 M KOH saturated with O_2 at a scan rate of 10 mV s^{-1}. The polarization curves before and after 500 cycles are shown in Fig. 7a. Almost no change was observed for the diffusion limiting current density by calculating the change values of the diffusion limiting current density of Fe-N-C/PGR (3:1) composites on ORR. It still remained 98.86% at −0.6 V after 500 cycles, demonstrating a high catalytic stability for the Fe-N-C/PGR (3:1) composites. To estimate the tolerance for the methanol to cross the catalysts, the Fe-N-C/PGR (3:1) composites and the commercial 20% Pt/C catalysts were studied by the chronoamperometry in 0.1 M KOH saturated with O_2 at a rotating speed of 1600 rpm and a scan rate of 10 mV s^{-1}. As shown in Fig. 7b, when the methanol was added at about 480 s, the current of the Fe-N-C/PGR (3:1) composites remained unchanged. However, an obviously decreased current was observed at the commercial 20% Pt/C catalysts with the presence of methanol. Thus, the Fe-N-C/PGR (3:1) composites had a better tolerance for the methanol to cross for ORR than the commercial 20% Pt/C catalysts.

Conclusions

In summary, a facile strategy for the synthesis of Fe-N-C/PGR ORR catalysts was developed by freeze-drying and pyrolysis, in which the FePc nanoclusters served as a source of abundant Fe-N-C active sites, and the GO was used as a precursor for 3D interpenetrating PGR to serve as support materials. It was found that by pyrolysis the FePc nanoclusters were easily converted into Fe-N-C nanoparticles

with lots of active sites on the surface of GR. The electrochemical measurements in alkaline conditions demonstrated that the Fe-N-C/PGR composites displayed a highly efficient catalytic activity, direct 4-electron selectivity, excellent stability, and better tolerance to methanol than the commercial 20% Pt/C catalysts toward ORR. The outstanding ORR performance of the Fe-N-C/PGR composites was contributed from the porous structure with high specific surface area, the formation of high density of Fe-N-C active sites and the synergistic effect between Fe-N-C active sites and PGR substrates. Therefore, the synthesized Fe-N-C/PGR catalysts can be a promising nonprecious candidate to replace commercial Pt/C catalyst for ORR in fuel cells. In addition, our facile synthetic process can be applied to construct other 3D graphene based materials especially composites or hybrid materials for energy or other related applications.[61–76]

ORCID

Zhanhu Guo ⓘ https://orcid.org/0000-0003-0134-0210

References

1. V. R. Stamenkovic, *Science*, **315**, 493 (2007).
2. E. M. Erickson, M. S. Thorum, R. Vasic, N. S. Marinkovic, A. I. Frenkel, A. A. Gewirth, and R. G. Nuzzo, *J. Am. Chem. Soc.*, **134**, 197 (2011).
3. L. M. Dai, Y. H. Xue, L. T. Qu, H. J. Choi, and J. B. Baek, *Chem. Rev.*, **115**, 4823 (2015).
4. D. Liu, X. Zhang, Z. Sun, and T. You, *Nanoscale*, **5**, 9528 (2013).
5. A. Zadick, L. Dubau, N. Sergent, G. Berthomé, and M. Chatenet, *ACS Catal.*, **5**, 4819 (2015).
6. M. K. Debe, *Nature*, **486**, 43 (2012).
7. L. Zhao, Y. Wang, and W. Li, *RSC Adv.*, **6**, 90076 (2016).
8. W. Li, D. Yang, H. Chen, Y. Gao, and H. Li, *Electrochim. Acta*, **165**, 191 (2015).
9. C. Li, X. Han, F. Cheng, Y. Hu, C. Chen, and J. Chen, *Nat. Commun.*, **6**, 7345 (2015).
10. B. B. Xiao, P. Zhang, L. P. Han, and Z. Wen, *Appl. Surf. Sci.*, **354**, 221 (2015).
11. W. Gu, L. Hu, W. Hong, X. Jia, J. Li, and E. Wang, *Chem. Sci.*, **7**, 4167 (2016).
12. P. J. Wei, G. Q. Yu, Y. Naruta, and J. G. Liu, *Angew. Chem. Int. Ed.*, **53**, 6659 (2014).
13. C. Zhang, R. Hao, H. Yin, F. Liu, and Y. Hou, *Nanoscale*, **4**, 7326 (2012).
14. K. Kaare, I. Kruusenberg, M. Merisalu, L. Matisen, V. Sammelselg, and K. Tammeveski, *J. Solid State Electrochem.*, **20**, 921 (2016).
15. R. Jasinski, *Nature*, **201**, 1212 (1964).
16. K. Wiesener, D. Ohms, V. Neumann, and R. Franke, *Mater. Chem. Phys.*, **22**, 475 (1989).
17. T. T. Tasso, T. Furuyama, and N. Kobayashi, *Inorg. Chem.*, **52**, 9206 (2013).
18. X. M. Hu, D. G. Xia, L. Zhang, and J. J. Zhang, *J. Power Sources*, **231**, 91 (2013).
19. X. Wang, B. Wang, J. Zhong, F. Zhao, N. Han, W. Huang, and Y. Li, *Nano Res.*, **9**, 1497 (2016).
20. Z. Chen, D. Higgins, A. Yu, L. Zhang, and J. Zhang, *Energy Environ. Sci.*, **4**, 3167 (2011).
21. L. Osmieri, R. Escudero-Cid, A. H. M. Videla, P. Ocón, and S. Specchia, *Appl. Catal. B: Environ.*, **201**, 253 (2017).
22. R. Zhang, Y. Peng, Z. Li, K. Li, J. Ma, Y. Liao, L. Zheng, X. Zuo, and D. Xia, *Electrochim. Acta*, **147**, 343 (2014).
23. Y. Jiang, Y. Xie, X. Jin, Q. Hu, L. Chen, L. Xu, and J. Huang, *RSC Adv.*, **6**, 78737 (2016).
24. H. A. M. Videla, L. Osmieri, M. Armandi, and S. Specchia, *Electrochim. Acta*, **177**, 43 (2015).
25. S. Yasuda, A. Furuya, Y. Uchibori, J. Kim, and K. Murakoshi, *Adv. Funct. Mater.*, **26**, 738 (2016).
26. X. Cui, S. Yang, X. Yan, J. Leng, S. Shuang, P. M. Ajayan, and Z. Zhang, *Adv. Funct. Mater.*, **26**, 5708 (2016).
27. M. Li, X. Bo, Y. Zhang, C. Han, and L. Guo, *J. Power Sources*, **264**, 114 (2014).
28. R. Cao, R. Thapa, H. Kim, X. Xu, M. G. Kim, Q. Li, N. Park, M. Liu, and J. Cho, *Nat. Comm.*, **4**, 2076 (2013).
29. X. Gao, J. Wang, Z. Ma, and J. Ye, *Electrochim. Acta*, **130**, 543 (2014).
30. Y. Jiang, Y. Lu, X. Lv, D. Han, Q. Zhang, L. Niu, and W. Chen, *ACS Catal.*, **3**, 1263 (2013).
31. Q. Jiang, L. Wang, C. Yan, C. Liu, Z. Guo, and N. Wang, *Eng. Sci.*, **1**, 64 (2018).
32. C. Lin, L. Hu, C. Cheng, K. Sun, X. Guo, Q. Shao, J. Li, N. Wang, and Z. Guo, *Electrochim. Acta*, **260**, 65 (2018).

33. C. Cheng, R. Fan, Z. Wang, Q. Shao, X. Guo, P. Xie, Y. Yin, Y. Zhang, L. An, Y. Lei, J. EunRyu, A. Shankar, and Z. Guo, *Carbon*, **125**, 103 (2017).
34. H. Hu, H. Liu, D. Zhang, J. Wang, G. Qin, and X. Zhang, *Eng. Sci.*, in press, (2018).
35. Y. He, S. Yang, H. Liu, Q. Shao, Q. Chen, C. Liu, and Z. Guo, *J. Colloid Interf. Sci.*, **517**, 40 (2018).
36. Z. Wu, S. Gao, L. Chen, D. Jiang, Q. Shao, B. Zhang, Z. Zhai, C. Wang, M. Zhao, Y. Ma, X. Zhang, L. Weng, M. Zhang, and Z. Guo, *Macromol. Chem. Phys.*, **218**, 1700357 (2017).
37. K. Sun, P. Xie, Z. Wang, T. Su, Q. Shao, J. Ryu, X. Zhang, J. Guo, A. Shankar, J. Li, R. Fan, D. Cao, and Z. Guo, *Polymer*, **125**, 50 (2017).
38. K. Zhang, G.-H. Li, L.-M. Feng, N. Wang, J. Guo, K.-X. Yu, J. B. Zeng, T. Li, and Z. Guo, *J. Mater. Chem. C*, **5**, 9359 (2017).
39. M. Zhao, L. H. Meng, L. C. Ma, L. Ma, X. B. Yang, Y. D. Huan, J. E. Ryu, A. Shankar, T. X. Li, C. Yan, and Z. H. Guo, *Compos. Sci. Technol.*, **154**, 28 (2018).
40. Y. Li, B. Zhou, G. Zheng, X. Liu, T. Li, C. Yan, C. Cheng, K. Dai, C. Liu, C. Shen, and Z. Guo, *J. Mater. Chem. C*, **6**, 2258 (2018).
41. Q. Luo, H. Ma, F. Hao, Q. Hou, J. Ren, L. Wu, Z. Yao, Y. Zhou, N. Wang, K. Jiang, H. Lin, and Z. Guo, *Adv. Funct. Mater.*, **42**, 1703068 (2017).
42. C. Wang, M. Zhao, J. Li, J. Yu, S. Sun, S. Ge, X. Guo, F. Xie, B. Jiang, E. Wujcik, Y. Huang, N. Wang, and Z. Guo, *Polymer*, **131**, 263 (2017).
43. X. Wang, X. Liu, H. Yuan, H. Liu, C. Liu, T. Li, C. Yan, X. Yan, C. Shen, and Z. Guo, *Mater. Design*, **139**, 372 (2018).
44. H. Liu, Y. Li, K. Dai, G. Zheng, C. Liu, C. Shen, X. Yan, J. Guo, and Z. Guo, *J. Mater. Chem. C*, **4**, 157 (2016).
45. C. Hu, Z. Li, Y. Wang, J. Gao, K. Dai, G. Zheng, C. liu, C. Shen, H. Song, and Z. Guo, *J. Mater. Chem. C*, **5**, 2318 (2017).
46. T. Liu, K. Yu, L. Gao, H. Chen, N. Wang, L. Hao, T. Li, H. He, and Z. Guo, *J. Mater. Chem. A*, **5**, 17848 (2017).
47. X. Fan, X. Chen, and L. Dai, *Curr. Opin. Colloid Interface Sci.*, **20**, 429 (2015).
48. C. Zhu, H. Li, S. Fu, D. Du, and Y. Lin, *Chem. Soc. Rev.*, **45**, 517 (2016).
49. H. Yin, C. Zhang, F. Liu, and Y. Hou, *Adv. Funct. Mater.*, **24**, 2930 (2014).
50. L. Yu, Y. Shen, and Y. Huang, *J. Alloys Compd.*, **595**, 185 (2014).
51. Y. Zhang, H. Liu, H. Wu, Z. Sun, and L. Qian, *Mater. Des.*, **96**, 323 (2016).
52. Y. Zhang, H. Wu, W. Zhao, X. Li, R. Yina, L. Qian, Y. Qi, and K. Yang, *Mater. Des.*, **130**, 366 (2017).
53. C. He, T. Zhang, F. Sun, C. Li, and Y. Lin, *Electrochim. Acta*, **231**, 549 (2017).
54. S. Brüller, H. W. Liang, U. I. Kramm, J. W. Krumpfer, X. Feng, and K. Müllen, *J. Mater. Chem. A*, **3**, 23799 (2015).
55. Q. Dong, X. Zhuang, Z. Li, B. Li, B. Fang, C. Yang, H. Xie, F. Zhang, and X. Feng, *J. Mater. Chem. A*, **3**, 7767 (2015).
56. M. Yang, H. B. Chen, D. G. Yang, Y. Gao, and H. M. Li, *J. Power Sources*, **307**, 152 (2016).
57. W. J. Jiang, L. Gu, L. Li, Y. Zhang, X. Zhang, L. J. Zhang, J. Q. Wang, J. S. Hu, Z. D. Wei, and L. J. Wan, *J. Am. Chem. Soc.*, **138**, 3570 (2016).
58. H. Schulenburg, S. Stankov, V. Schünemann, J. Radnik, I. Dorbandt, S. Fiechter, P. Bogdanoff, and H. Tributsch, *J. Phys. Chem. B*, **107**, 9034 (2003).
59. B. Liu, B. Huang, B. Lin, J. Ye, and L. Ouyang, *Appl. Surf. Sci.*, **411**, 487 (2017).
60. D. Higgins, P. Zamani, A. Yu, and Z. Chen, *Energy Environ. Sci.*, **9**, 357 (2016).
61. T. Su, Q. Shao, Z. Qin, Z. Guo, and Z. Wu, *ACS Catalysis*, **8**, 2253 (2018).
62. L. Dashairya, M. Rout, and P. Saha, *Adv. Compos. Hybrid Mater.*, **1**, 135 (2018).
63. B. Song, T. Wang, H. Sun, Q. Shao, J. Zhao, K. Song, L. Hao, L. Wang, and Z. Guo, *Dalton Trans.*, **46**, 15769 (2017).
64. C. Lin, H. Hu, C. Cheng, K. Sun, X. Guo, Q. Shao, J. Li, N. Wang, and Z. Guo, *Electrochim. Acta*, **260**, 65 (2018).
65. J. Huang, Y. Cao, Q. Shao, X. Peng, and Z. Guo, *Ind. Eng. Chem. Res.*, **56**, 10689 (2017).
66. X. Wang, X. Zeng, and D. Cao, *Eng. Sci.*, **1**, 55 (2018).
67. Q. Luo, H. Ma, Q. Hou, Y. Li, J. Ren, X. Dai, Z. Yao, Y. Zhou, L. Xiang, H. Du, H. He, N. Wang, K. Jiang, H. Lin, H. Zhang, and Z. Guo, *Adv. Func. Mater.*, **28**, 1706777 (2018).
68. H. Kang Z. Cheng et al., *Separation Purification Technol.*, **201**, 193 (2018).
69. H. Du, C. Zhao, J. Lin, Z. Hu, Q. Shao, J. Guo, B. Wang, D. Pan, E. K. Wujcik, and Z. Guo, *Chem. Rec.*, in press.
70. Z. Hu, Q. Shao, Y. Huang, L. Yu, D. Zhang, X. Xu, J. Lin, H. Liu, and Z. Guo, *Nanotechnology*, **29**, 185602 (2018).
71. K. Sun, R. Fan, X. Zhang, Z. Zhang, Z. Shi, N. Wang, P. Xie, Z. Wang, G. Fan, H. Liu, C. Liu, T. Li, C. Yan, and Z. Guo, *J. Mater. Chem. C*, **6**, 2925 (2018).
72. Q. Luo, H. Chen, Y. Lin, H. Du, Q. Hou, F. Hao, N. Wang, Z. Guo, and J. Huang, *Adv. Func. Mater.*, **27**, 1702090 (2017).
73. W. Deng, T. Kang, H. Liu, J. Zhang, N. Wang, N. Lu, Y. Ma, A. Umar, and Z. Guo, *Sci. Adv. Mater.*, **10**, 937 (2018).
74. Y. Guo, G. Xu, X. Yang, K. Ruan, T. Ma, Q. Zhang, J. Gu, Y. Wu, H. Liu, and Z. Guo, *J. Mater. Chem. C*, **6**, 3004 (2018).
75. C. Wang, Z. He, X. Xie, X. Mai, Y. Li, T. Li, M. Zhao, C. Yan, H. Liu, E. Wujcik, and Z. Guo, *Macromol. Mater. Eng.*, **3**, 1700462 (2018).
76. F. Pan, X. Xiang, and Y. Li, *Eng. Sci.*, **1**, 21 (2018).